Journal of Mines, Metals and Fuels, 71(2): 186-195; 2023. DOI: 10.18311/jmmf/2023/.....

Print ISSN : 0022-2755

Journal of Mines, Metals and Fuels

Contents available at: www.informaticsjournals.com/index.php/jmmf

Performance Evaluation of Hypersonic Flow Past Blunt Bodies with Aerospikes using Numerical Techniques

Syed Mohammed Musharraf and Srinivas G*

*Department of Aeronautical and Automobile Engineering, Manipal Institute of Technology, Manipal Academy of Higher Education (MAHE), Manipal, Udupi, Karnataka, India 576104. *E-mail: srinivas.g@manipal.edu*

Abstract

The majority of hypersonic vehicle designs focus on reducing drag and controlling flow enthalpy. Aerodynamic drag is caused by high surface pressure, which creates a detached bow shock in ahead of the blunt nose. These flow separation bow shocks impact hypersonic vehicle speed, range, and heating. Converting the detached shockwave to an attached shock wave (family of the weaker shock) and keeping the dissipation area large enough for a higher heat dissipation rate is a straightforward way to solve aerothermodynamics problems. The most popular technique involves introducing an antenna-like structure known as an Aerospike, placed right at the stagnation point over the blunt head. The aerospike contributes to the generation of the attached shock wave, which reduces the pressure drag component and results in recirculation zones over of the nose. This paper evaluates the performance of an aerospike hypersonic vehicle under various off-design conditions using the ANSYS Fluent software. Flow simulations are validated with available experimental data and tested under various turbulence models. All numerical simulations of the vehicle with aerospike are studied in detail, including flow properties such as pressure, temperature, density, turbulence model, etc. The paper concluded that drag reduction results under specific flow conditions were achieved by incorporating the aerospike into the hypersonic vehicle. Furthermore, this paper also contributes to the future research field of hypersonic aeromechanical engineering.

Keywords: *Aerospike, Computational fluid dynamics (CFD), Drag reduction, shock wave, recirculation zones.*

1.0 Introduction

Hypersonic flows are not just about the flow speed or Mach number. The properties in this regime change rapidly, unlike the supersonic and subsonic flow regimes. Hence the designing perspective focuses mainly on the drastic change in aerodynamic drag and heat or flow enthalpy. To release the heat produced, the nose of these vehicles are kept in a blunt shape which increases the surface area to dump the heat into the air. However, these brunt nose shapes generate a detached bow shock wave leading to a higher drag value. This high-pressure wave results in a pressure drag, which affects the vehicle's performance. The drag is a quantity which cannot be ignored. A trade was made where the heat liberation was given higher importance over the aerodynamic drag. However, the issue of aerodynamic drag had to be addressed for smooth and efficient functioning of the vehicle. A straightforward way to solve aerothermodynamics problems was by converting the detached shock wave into an attached shock wave (family of the weaker shock), keeping the dissipation area large enough. The most popular and effective technique involves introducing an antenna-like structure known as an aerospike, placed over the stagnation point of the blunt head. The main focus of current research

*Corresponding Author

will be on assessing the performance of a blunt body past hypersonic flows using the different CFD methods.

The aerospike effectively contributes to the overall drag reduction. Aerospikes contribute to the attached shock wave generation, which reduces the pressure drag component and results in re-circulation zones in front of the body. The re-circulation zone results in the decrease of pressure along with wall flux in the blunt nose area (after hitting the spike tip), reducing aerodynamic drag and heating. The low drag value indicates the enhanced and efficient performance of the vehicle. Studys show that these spikes can be used for any other operational uses such as a flight speed measuring pitot tube or gas sample collector and others.

2.0 Literature Review

2.1 Studies Done to Date

Lockheed-Martin's Trident-I missile stood among the initial vehicle to adopt the aerospikes. In hypersonic flows, these aerospikes were found to have drag reduction up to 52%. The era of the aerospike began when Alexander mentioned in his paper [19]. He used the term conical windshield, which had a 27% lower drag coefficient than the blunt nose. Pilan and Putlan first used the term spike in their paper (Robert Piland et al., 1954). Thus, began the studies and experiments on aerospike. The effect of spike length and length to diameter was put forward by (Mair, 1952). The wind tunnel experimentations on aerospikes over different flow conditions began to find efficient geometric data to prove its effectiveness.

(Khurana & Suzuki, 2013) conducted an experimental study on a lifting body configuration for a Mach number of 7 in which they stated that aerodynamic efficiency and longitudinal stability were strongly influenced by characteristics like the shape and length of the aerospike mounted. (Huebner et al., n.d.) performed tests on the effectiveness and feasibility of these aerospikes at Mach 6. Using the aerospikes with aero-disk at an angle of attack 5^{o} at the given flow condition was beneficial. With the spike ON state, the separation shock impingement was found on the dome at a higher angle of attack. They also discovered that the existence of the collar on the dome creates small flow circulation regions, causing an increase in temperature and stabilising the pressure along the surface. (Kalimuthu2008, n.d.) stated that the shock wave moved further away from the blunt-body as the L/D ratio increased because of the re-circulation region. The most effective length to diameter ratio (L/D) found was 2.0. The shear-layer separation and the shock re-compression resulting from the re-attachment point are visible.

(Sebastian et al., 2016) stated that along with drag reduction, the lift coefficient increased at the lower angle of attack. It was later on numerically simulated with multiple shapes, including hemispherical and triangular shapes. The hemispherical tip resulted in a 4% drag force reduction, and the triangular spike decreased by 3.6% drag force compared to the base model.

2.2 literature Review Summary

Different studies were conducted to see the effectiveness of these aerospikes. The aerospikes were analysed with varying flow conditions, speed, antenna length, and materials.

- The drag force of the geometry changed with the angle of attack and the L/D ratio. Some studies have proved that the higher the length to the diameter ratio, the higher the drag reduction.
- The drag is reduced by the re-circulation region formed by stagnation pressure around the blunt nose part.

2.3 Research Gap

Most numerical simulation studies were carried out using the K epsilon model. The flow speed mainly was chosen to be Mach no.6. In the current study, an attempt was made to perform the numerical simulation with other turbulence models like k omega SST over various flow speed Mach numbers.

3.0 Objectives

- Firstly, is to validate the aerodynamic prospect of using an aerospike using the current research study. To deduce whether the addition of the aerospike will resolve the drag reduction problem.
- To know how the flow pattern and aerodynamics of the existing body change with the addition of this aerospike. To explore the outcome when dimensions of the aerospike differed each time.
- Comparing the outcome of the coefficient of drag value with and without spike condition. To study the rag reduction scenario over different turbulence models and varied boundary conditions

4.0 Governing Equations

The current numerical analysis is performed using CFD (Computational Fluid Dynamics). CFD is an analysis tool that uses mathematical equations to accurately predict the fluid flow pattern, heat transfer rate and other many phenomena. These mathematical equations are derived from the basic

principles of the Law of conservation of mass given by equation (1), the Law of conservation of energy given by equations (2a), (2b) and (2c), and the Law of conservation of momentum given by equation (3). The governing equations derived from these laws are,

(i) Equation of Continuity

$$\partial\rho/\partial t + \nabla \cdot(\rho^*V) = 0 \quad \text{... (1)}$$

(ii) Equation of Momentum

$$\partial(\rho^*u)/\partial t + \nabla \cdot(\rho^*u^*V) = -\partial p/\partial x + \rho\, fx + (Fx)_{viscous} \quad \text{... (1a)}$$

$$\partial(\rho^*v)/\partial t + \nabla \cdot(\rho^*v^*V) = -\partial p/\partial y + \rho^*fy + (Fy)_{viscous} \quad \text{... (1b)}$$

$$\partial(\rho^*w)/\partial t + \nabla \cdot(\rho^*w\,V) = -\partial p/\partial z + \rho^*fz + (Fz)_{viscous} \quad \text{... (1c)}$$

(iii) Equation of Energy

$$\partial/\partial t[\rho(e + V^2/2)] + \nabla\cdot[\rho(e + V^2/2)\,V] = \rho^*q^{\cdot} - \nabla\cdot(p^*V) + \rho(f\cdot V) + Q^{\cdot}_{viscous} + W^{\cdot}_{viscous} \quad \text{... (3)}$$

These equations put together are called Navier Stokes Equations. One such method of CFD in Ansys Fluent is the Reynolds Averaged Naiver Stokes equations model (RANS). This model solves the averaged flow using the Navier Stokes equation. We approximate the effect of turbulence on the mean flow by different Turbulence Models. The Navier Stokes equation is given by equations (4a) and (4b) as shown,

$$\nabla . u = 0 \quad \text{... (4a)}$$

$$(Du/Dt) = -\nabla p + \mu\nabla^2 u + f \quad \text{... (4b)}$$

The LHS represents the local and convective acceleration, whereas the RHS represents the pressure gradient, body force, and viscous effect terms.

Where,

V – velocity

ρ – fluid density

f – body force per unit mass

e – internal energy

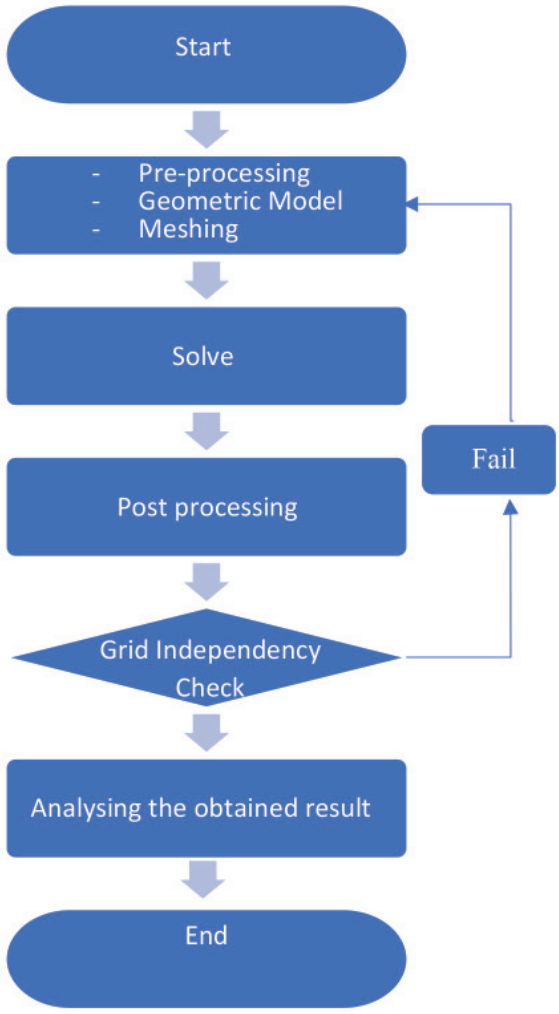
q – heat added

p – pressure

5.0 Methodology

5.1 Work Flow

The numerical study was performed as per the reference papers (Mansour & Khorsandi, 2014; Sebastian et al., 2016) for validation. A similar result obtained confirmed the precision of the chosen method. This model was then studied with the changed boundary conditions and turbulence model. The grid independency check verified the required discretisation for an efficient and computational power saving process. The flow chart below explains the stepwise process involved;



Flow chart – Stepwise process for the current study

The study will be carried out in two different parts.

- Without the spike
- With the aerospike

Since the simulations aim to compare the final result and deduce the obtained drag reduction, the steps are repeated for both cases. Later on, to find the appropriate turbulence model, the initial modelling operation was done on the software CATIA V5. Later, the discretisation and numerical simulation were carried out in software Ansys 2020R1 under the Fluent workbench.

5.2 Geometry

The considered geometry is as shown in the figure. The model is a cylinder with a hemispheric dome shape on the side. The considered diameter of the cylinder/hemisphere is D which is 40mm, and the length of the cylindrical side is 1.25D. The aerospike which was considered for the study is

mounted over the hemisphere. Again, this spike consists of the cylindrical part and hemisphere nose-mounted over the side. The diameter of this cylindrical/hemispheric part is 0.1D. The length is varied for two cases based on the length to diameter ratio (L/D), which is 1.5 and 2. The final geometry is shown in Figures 1 and 2.

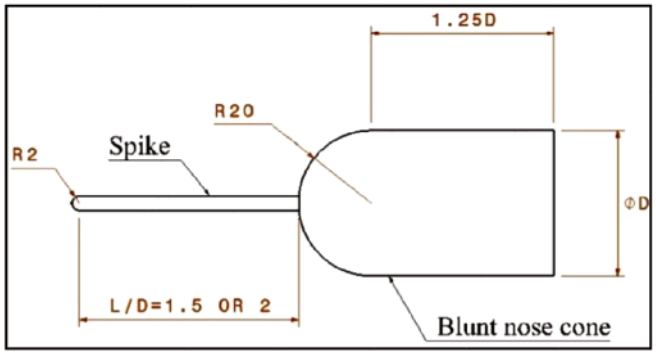


Figure 1: Geometry used in the current study as per (Sebastian et al., 2016)

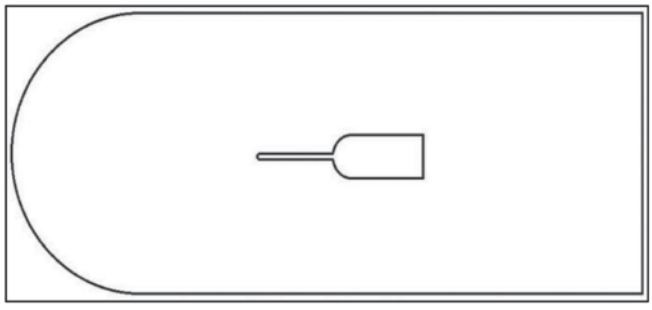


Figure 2: Flow field of the model in the current study as per (Sebastian et al., 2016)

5.3 Grid Generation

In the present 2D axis-symmetric model, the unstructured grid type was applied. The density of the elements was higher surrounding the body to record the boundary layer and shear layer formed due to viscous interactions and the formation of the re-circulation region. The grid generated is as shown in Figures 3 and 4. The mesh element density was coarse as we move further away from the body. This coarse nature will help in reducing the computational time. Inflation layers were added to observe the high-definition shock wave contours.

A grid independency test was performed using different element sizes to find the most effective mesh elements count. One such case is shown in Table 1.

Based on the Test conducted, the appropriate number of elements was 135370 to save computational power.

Table 1: Grid Independency test results

No of elements	Cd value	Drag reduction	Variation
10230	0.414	55%	8.6%
135370	0.435	52.1%	0%
209470	0.438	51.8%	3.3%
526710	0.438	51.8%	3.3%

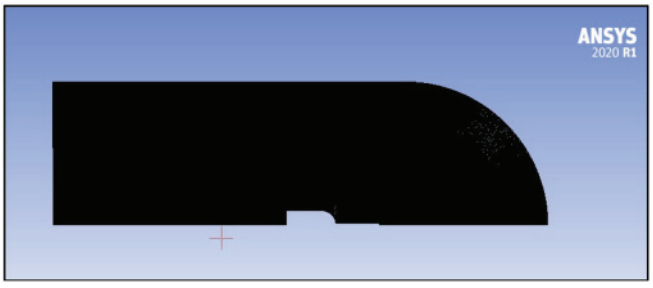


Figure 3: Fine un-structured Mesh generation

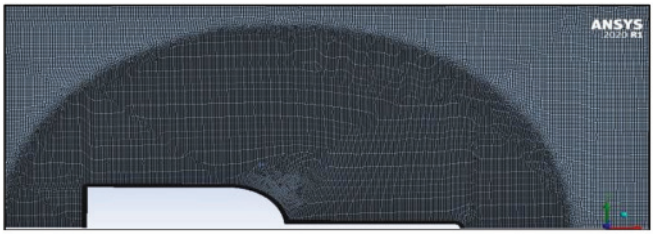


Figure 4: Inflation layers were added to capture near-wall flow circulation

5.4 Fluent Flow Solver

The current study is a steady case since the flow field converged at the steady-state case. The local time-stepping option used by steady-state conditions contributes to faster convergency. The density-based solver option was checked to enable the Navier stokes couples solution algorithm. The current study involves compressible flows, so ideal gas equations are turned ON. The viscosity is computed using the Sutherland law given by equation (5). This Law helps in establishing a proper relation between the dynamic viscosity and the temperature.

$$\mu = \mu_0((T/T_0)^{3/2}*(T_0+S))/(T+S) \quad \text{... (5)}$$

Where,

μ = viscosity

T = static temperature

μ_0 (reference value) = 1.716×10^5 kg/m-s

S (effective temperature) = 110.56K

T_0 (reference temperature) = 273.11K

The implicit scheme for velocity coupling is preferred for compressible flow simulations as it is stable for linear systems. The second order upwind- interpolation scheme was applied to solve the convective terms.

5.4.1. Turbulence model

Reynolds Averaged Navier Stokes (RANS) will be used for the current simulations. For the initial computational analysis and validation, two-equation, the standard K-epsilon model was used. Many researchers in their study have extensively selected this model. The K-epsilon model is re-known for its accuracy over a wide rangeof flows. The underlying turbulent kinetic energy and turbulence dissipation rate are given as the equations (6), (7) and (8);

The equation for Turbulence Kinetic Energy (k):

$$D/Dt\,(\rho^*k) = \nabla\cdot(\rho^*Dk^*\nabla k) + P - \rho^*\epsilon \quad \ldots (6)$$

$$\partial/\partial t(\alpha^*\rho^*k) + \nabla\cdot(\alpha^*\rho^*\mathbf{u}^*k) - \nabla^2(\alpha^*\rho^*Dk^*k) = \alpha^*\rho^*G - (2/3\alpha^*\rho^*\nabla\cdot uk) - (\alpha^*\rho(\epsilon/k)k) + Sk + S^*fv^*Options \quad \ldots (7)$$

The Turbulence Dissipation (epsilon):

$$D/Dt\,(\rho^*\epsilon) = \nabla\cdot(\rho^*D\epsilon^*\nabla^*\epsilon) + C1^*\epsilon/k\,(P + C32/3\,k\nabla\cdot u) - C2^*\rho(\epsilon^2/k) \quad \ldots (8)$$

Where,

K = Turbulent KE

D_k = diffusivity (effective) for the turbulent KE

P = Turbulent KE production rate

ε = Turbulent KE dissipation rate

D_ε = Effective diffusivity for ε

C_1 = Model-coefficient

C_2 = Model-coefficient

S_k = Internal source term for K

$S_{fvOptions}$ = Source terms introduced by fvOptions dictionary for K

The current study was extended with the numerical simulation using the 2 equation K-omega SST model. This model is re-known for its accurate prediction of the flow pattern including the boundary layer flows having strong pressure gradient and flows separation at supersonic and hypersonic speeds. The underlying turbulent kinetic energy equation is (6) and (7), which was used earlier, and the specific dissipation rate is given by equation (9) below.

The specific dissipation rate (omega):

$$D/Dt(\rho^*\omega) = \nabla\cdot(\rho^*D\omega\nabla\omega) + (\rho^*\gamma^*G)/\nu - (2/3\rho^*\gamma^*\omega\,(\nabla\cdot u)) - (\rho^*\beta^*\omega^2) - \rho^*(F1-1)CD^*k_\omega + S\omega, \quad \ldots (9)$$

5.4.2. Boundary conditions

The boundary conditions were chosen according to the research done by (Sebastian et al., 2016)

Table 2: Stagnation Boundary Conditions as per (Sebastian et al., 2016)

Angle of Attack	0
P_0	8.3 MPa
T_0	450K
Ma	6

This was converted into the free stream conditions at Ma = 6 using the isentropic equations which are (10), (11) and (12).

$$T_0/T = 1 + ((\gamma - 1)/2)\,M^2 \quad \ldots (10)$$

$$P_0/P = (1 + ((\gamma - 1)/2)\,M^2)^{\gamma/\gamma-1} \quad \ldots (11)$$

$$\rho_0/\rho = (1 + ((\gamma - 1)/2)\,M^2)^{1/\gamma-1} \quad \ldots (12)$$

Hence the freestream static conditions turned out to be as shown in Table 3.

Table 3: Static Boundary Conditions

Angle of attack	0
P	525.688 Pa
T	K
Ma	6

The inlet, outlet, and the surroundings were selected as Pressure Fairfield conditions. The inner model was given to be the wall condition with 300K as the wall temperature. The operating pressure condition was set to zero.

For further study, the turbulence models have been varied with varied boundary conditions. The varied boundary conditions allow us to observe the flow field over a broad range of conditions. Table 4 consists of the new boundary conditions that would help us understand and improve aerodynamics.

Table 4: New Boundary Conditions

Property	Varied BCs -1	Varied BCs - 2
Static pressure	892.1006	319.932
Static temperature	63.83	47.62
Mach number	5.5	6.5

6.0 Results and Inspection

The flow over the blunt body was numerically simulated. The results show the existence of a strong detached bow shock generated at a standoff distance from the hemispheric nose. The stagnation pressure was found to be very high.

The simulation is performed again with the presence of the aerospike over the blunt nose. The addition of this spike generates an attached shock wave with a weaker stagnation pressure region upstream. A flow re-circulation zone and the shear boundary layer separation were observed ahead of the blunt part.

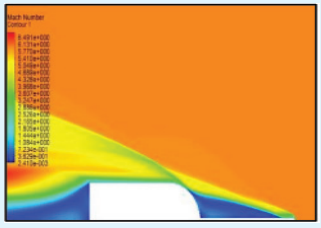
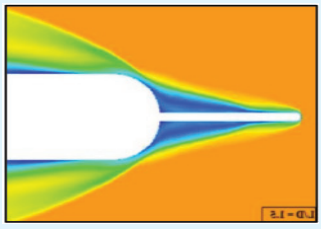
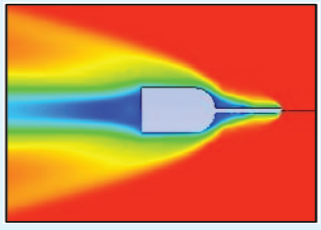
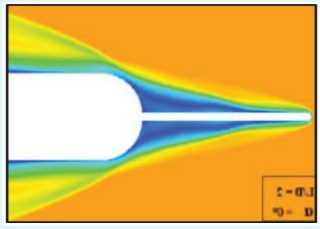
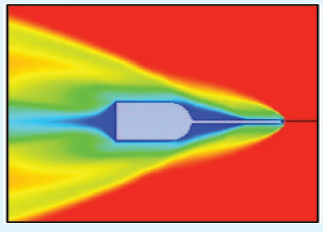
6.1 Drag Reduction

The drag coefficient for both cases was simulated and calculated using the equation (13). The obtained results from

Table 5: Results comparison between current obtained results and (Mansour & Khorsandi, 2014; Sebastian et al., 2016)

Condition	Cd as per (Mansour & Khorsandi, 2014)	Cd as per (Sebastian et.al 2016)	Cd found in simulation	Percentage error concerning (Mansour & Khorsandi, 2014)	Percentage error concerning (Sebastian et.al 1016)
No spike	0.95	0.91	0.92	4.2%	1%
Spike when L/D = 1.5	0.58	0.37	0.49	15.5%	24.4%
Spike when L/D = 2	-	0.24	0.25	-	4%

Table 6: Contours comparison between the current simulations and work done by (Mansour & Khorsandi, 2014; Sebastian et al., 2016)

Property	As per (Mansour and Khorsandi, 2014)	As per (Sebastian et al., 2016)	Current simulations
Mach number L=1.5			
Mach number L = 2	-		

the spike conditions indicate the drag reduction.

$C_d = D\ F/q_{ef}\ S$ ... (13)

DF = the drag force, (found from the analysis.)

q_{ref} = the dynamic reference-pressure

(defined by $1/2(\rho_{ref} * v^2_{ref})$)

in which;

ρ_{ref} = the reference-density and

v_{ref} = the reference-velocity

S = the reference-area of the cylindrical diameter

The results obtained from different research journals and current research will be shown in the next segment

6.2 Baseline Results

The geometry with no spike showed the maximum Cd value as expected. The addition of the aerospike proved to be useful as it showed the drag reduction in the final value. Table 5 compares the results obtained during the current numerical simulation (Mansour & Khorsandi, 2014; Sebastian et al., 2016). The error percentage was found to be high.

6.2.1 Validation

The baseline analysis results were identically close to the reference study. The data was found to be deviating from the original data with a smaller margin. This deflection can be assumed because of the dimensional assumptions or minor digression in input boundary conditions.

The results obtained after varying the boundary conditions and the turbulence model are shown.

6.3 Modified Results

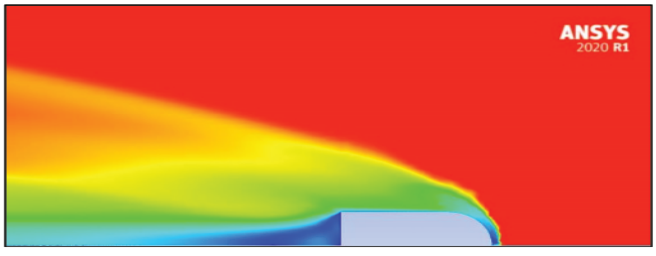


Figure 5 Mach number contour of the no-spike body

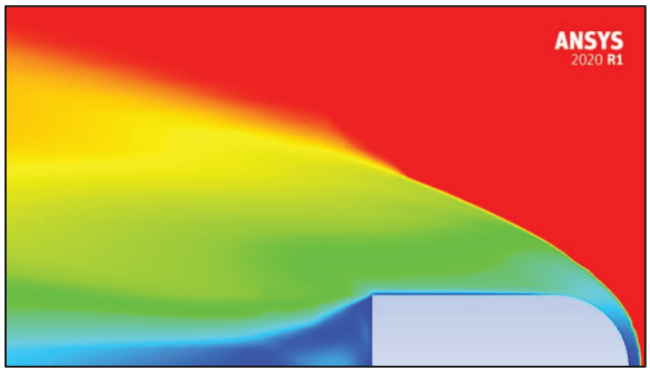


Figure 6 Mach number contour with Varied Boundary condition

A. With Initial Boundary Conditions

(i) L = 1.5

Table 7: Results obtained with Initial BCs for L=1.5

T M	Cd of the no spike condition	Cd with spike ON	Drag reduction %
K – ε	0.92	0.49	46.7%
K – ω SST	0.91	0.43	53.74%

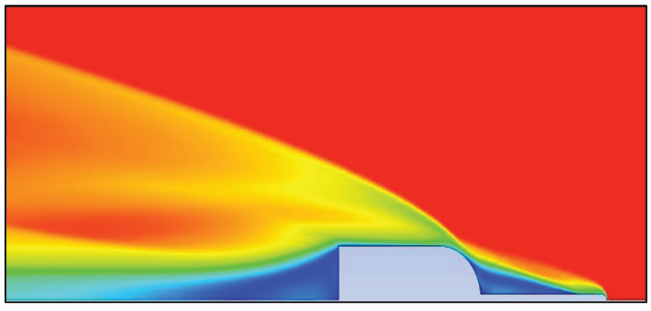


Figure 7: Mach number contour of L=1.5 K-omega Turbulence model

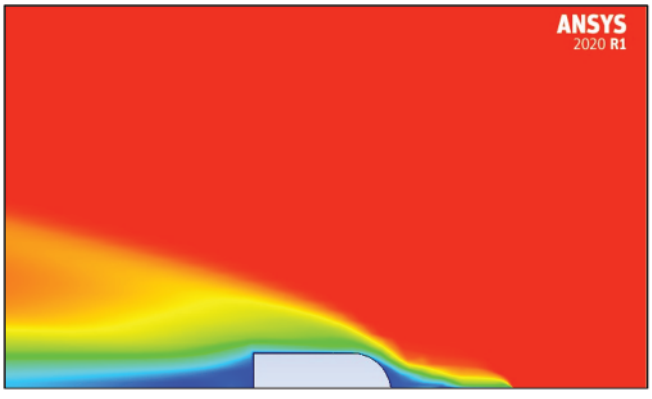


Figure 8: Mach number contour of L=1.5 K-epsilon turbulence model

(ii) L = 2

Table 8: Results obtained with Initial BCs for L=2

Turbulence Model	Cd of the no spike condition	Cd with spike ON	Drag reduction percentage
K–epsilon	0.92	0.25	72.8%
K–omega SST	0.91	0.23	74.7%

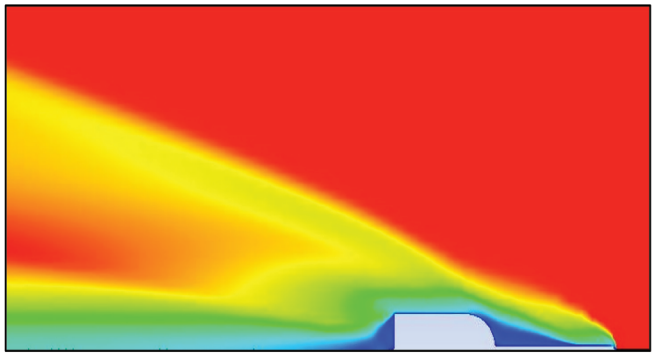


Figure 9: Mach number contour of L=2 K-omega turbulence model

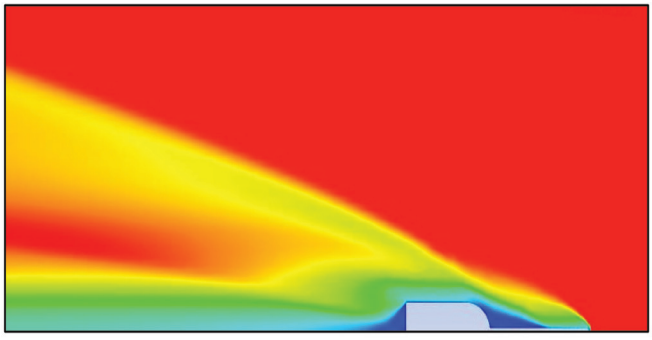


Figure 10: Mach number contour of L=2 K-epsilon turbulence model

B. Varied Boundary Condition 1

(i) L = 1.5

Table 9: Results obtained with Varied BCs-1 for L=1.5

T M	Cd of the no spike condition	Cd with spike ON	Drag reduction percentage
K-ε	0.92	0.82	10%
K-ω SST	0.91	0.44	51.6%

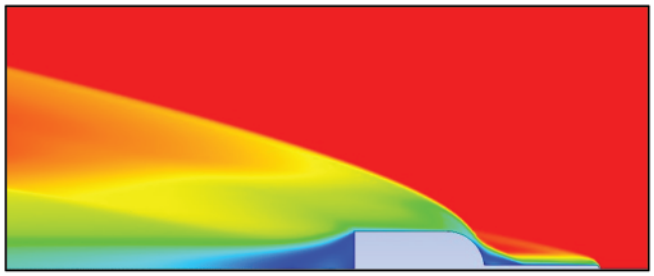


Figure 11 Mach number contour of L=1.5 K-epsilon turbulence model with BC2

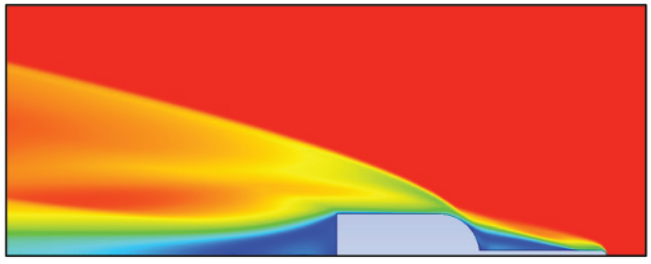


Figure 12 Mach number contour of L=1.5 K-omega turbulence model with BC2

(ii) L = 2

Table 10: Results obtained with Varied BCs-1 for L=2

T M	Cd of the no spike condition	Cd with spike ON	Drag reduction percentage
K-ε	0.92	0.69	25%
K – ω SST	0.91	0.42	53.8%

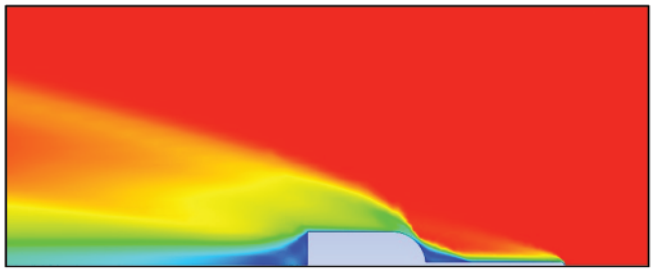


Figure 13 Mach number contour of L=2 K-epsilon turbulence model with BC2

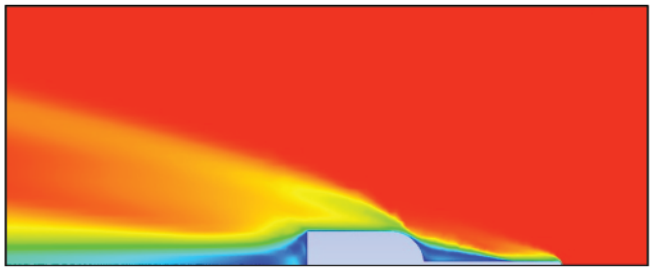


Figure 14 Mach number contour of L=2 K-omega turbulence model with BC2

C)Varied Boundary Condition 2

(i) L = 1.5

Table 11: Results obtained with Varied BCs-2 for L=1.5

T M	Cd of the no spike condition	Cd with spike ON	Drag reduction percentage
K- ε	0.92	0.81	10%
K – ω SST	0.93	0.419	55%

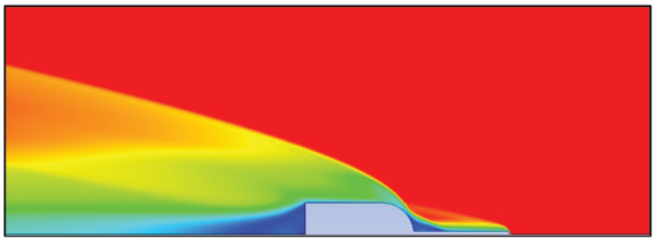


Figure 15 Mach number contour of L=1.5 K-epsilon turbulence model with BC3

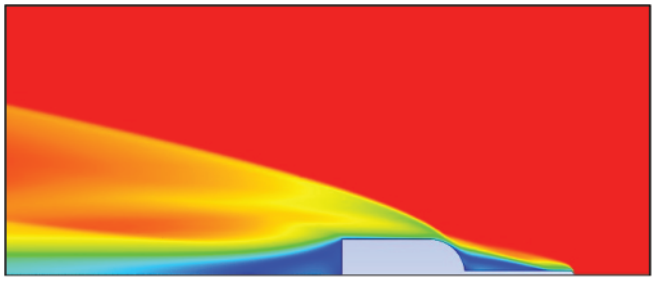


Figure 16 Mach number contour of L=1.5 K-omega turbulence model with BC3

(ii) L = 2

Table 12: Results obtained with Varied BCs-2 for L=2

T M	Cd of the no spike condition	Cd with spike ON	Drag reduction percentage
K-ε	0.92	0.68	26%
K–ω SST	0.93	0.40	57%

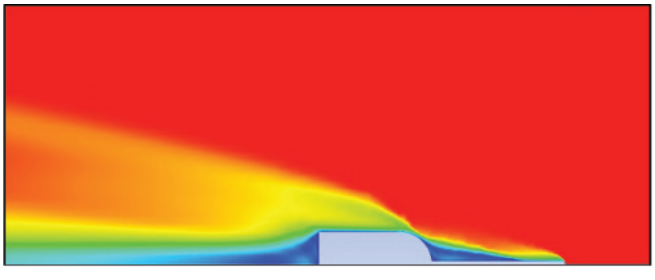


Figure 17: Mach number contour of L=2 K-omega turbulence model with BC3

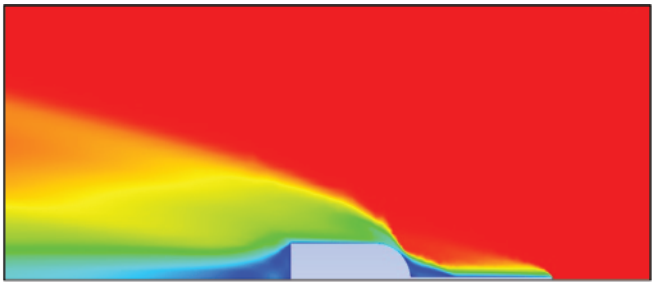


Figure 18: Mach number contour of L=2 K-epsilon turbulence model with BC3

The drag reduction percentage is higher when using the turbulence model *K*-omega SST. Another notable observation was that the flow contours were different for different turbulence models. The flow separation occurred sooner in the *K*-omega SST model than in the *K*-epsilon model. However, comparing the experimental results and figures, the contours of the *K*-omega SST model were close to accurate.

7.0 Conclusions

The experimental results show significant drag reduction in blunt-body on the addition of the aerospike. It was observed that the coefficient of drag value changes with change in the geometrical condition. In this study, a 3d model of a blunt body with aerospike mounted over top was analysed. The effectiveness of these aerospikes found after numerous experimental studies were compared to the numerical analysis result. The hypersonic flow visualisation at Mach numbers 5.5, 6, 6.5 over without and with aerospikes with L/D ratios 1.5 and 2 was numerically simulated. The turbulence model *k* epsilon and *k* omega were also varied. The Drag value decreased as the aerospikes were added to the blunt-body geometry. The drag reduction value was higher for L/D=2 than 1.5. The primary reason for the drag reduction was the re-circulation zone formed ahead of the blunt nose. The detached shockwave transformed into an attached shock wave generating lower stagnation pressure upstream. It is crucial to choose the correct turbulence model in the numerical investigation study. Using the *k*-epsilon turbulent model, the flow detachment was delayed over a larger spike distance than the *k*-omega turbulence model. It is found that the *K*-omega turbulence model provides the closest possible solution to the experimental results. The variation in the value of the drag coefficient over the given flow condition was minimal.

Hence, the aerospike does prove its effectiveness over varied boundary conditions and turbulence models. The simulations conducted merely proves the theoretical validity and can vary from the actual performance. The drag reduction obtained is considerable and can be utilised in space crafts with proper optimisation.

The present computational geometric model is being studied for further development. This might lead to discovery of new highly optimised drag-reduction devices for high-speed flows.

8.0 Acknowledgements

I express my gratitude to my professor Dr. G Srinivas, for his constant guidance and support in finishing my research and giving the form of this paper. I would also like to thank Manipal Academy of Higher Education, for providing me with such a wonderful opportunity as a student in the Aeronautical and Automobile Engineering department.

In the end, I would like to thank my parents for supporting me in every step of the career decisions I took in my life.

9.0 References

[1] Ahmed, M. Y. M. and Qin, N. (2011): Recent advances in the aerothermodynamics of spiked hypersonic vehicles. In Progress in Aerospace Sciences (Vol. 47, Issue 6, pp. 425–449). Elsevier Ltd. https://doi.org/10.1016/j.paerosci.2011.06.001

[2] Aliaga, C., Guan, K., Selvanayagam, J., Stokes, J., Viti, V., and Menter, F. (2020): Hypersonic applications of the laminarturbulent transition SST model in ANSYS fluent. AIAA Aviation 2020 Forum, 1 PartF. https://doi.org/10.2514/6.2020-3290

[3] Asif, M., Zahir, S., Kamran, N. and Khan, M. A. (2004): Computational Investigations Aerodynamic Forces at Supersonic/ Hypersonic Flow past a Blunt Body with various Forward Facing Spikes.

[4] Bogdonoff, S. M., and Vas , I. E. (1959): Preliminary Investigations of Spiked Bodies at Hypersonic Speeds. *Journal of the Aerospace Sciences*, 26(2), 65–74. https://doi.org/10.2514/8.7945

[5] Deng, F., Xie, F., Qin, N., Huang, W., Wang, L., and Chu, H. (2018): Drag reduction investigation for hypersonic lifting-body vehicles with aerospike and long penetration mode counterflowing jet. *Aerospace Science and Technology,* 76, 361–373. https://doi.org/10.1016/j.ast.2018.01.039

[6] Feszty, D., Richards, B. E., Badcock, K. J., and Woodgate, M. A. (2000a): Numerical simulation of a pulsating flow arising over an axisymmetric spiked blunt body at Mach 2.21 and Mach 6.00. In Shock Waves.

[7] Gupta, D. (2017): *International Journal of Research In Aeronautical and Mechanical Engineering*

Divyang Gupta Drag Reduction of Hypersonic Vehicles using aerospike.

[8] Han, R., Liu, W., Yang, X., and Chang, X. (2021): Dynamic Drag Reduction Effects of Aerospikes and Aerodisks. *International Journal of Aerospace Engineering, 2021*. https://doi.org/10.1155/2021/9370331.

[9] Huebner, L. D., Mitchell, A. M., and Oudreaux, E. J. (n.d.). Experimental Its on the Feasibility of an Aerbspike for ersonic.

[10] Sidney R. Alexander. (1953): Results of Tests to Determine The Effect of A Conical Windshield on The Drag of a Bluff Body at Supersonic Speeds. NACA Resarch Abstracts, 2.

[11] Kalimuthu, R. and Rathakrishnan, E. (2008): Aerospike for Drag Reduction in Hypersonic Flow

[12] Khurana, S. and Suzuki, K. (2013): Assessment of aerodynamic effectiveness for aerospike application on hypothesised lifting-body in hypersonic flow. 31st AIAA Applied Aerodynamics Conference. https://doi.org/10.2514/6.2013-2513

[13] Kim, H. and Lee, M. (2021): Flow simulation of a supersonic airplane with installed engine nacelle. *Aerospace Science and Technology*, 117. https://doi.org/10.1016/j.ast.2021.106900

[14] Mair, W. A. (1952a): LXVIII. Experiments on separation of boundary layers on probes in front of blunt-nosed bodies in a supersonic air stream. *The London, Edinburgh, and Dublin Philosophical Magazine and Journal of Science*, 43(342), 695–716. https://doi.org/10.1080/14786440708520987

[15] Mansour, K. and Khorsandi, M. (2014): The drag reduction in spherical spiked blunt body. *Acta Astronautica*, 99(1), 92–98. https://doi.org/10.1016/j.actaastro.2014.02.009

[16] Mehta, R. C. (2009): Flow Field Computations Over Conical, Disc and Flat Spiked Body at Mach 6.

[17] Miliæev, S. S. and Pavloviæ, M. D. (2002): Influence of spike shape at supersonic flow past blunt-nosed bodies: Experimental study. *AIAA Journal*, 40(5), 1018–1020. https://doi.org/10.2514/2.1745

[18] N, S. S. (2013): Numerical Analysis of Aero-Spike Nozzle for Spike Length Optimization. 1, 1–14.

[19] Results of Tests of Determine the Effect of. (n.d.).

[20] Robert Piland, B. O., P utland, L. W. and Putland, L. W. (1954): I-RM L54A27 ZE Ro-Lift Drag of Seve Ral Conical and Blunt Nose Shapes Obtained In F Re E F Light At Mach Numbers of 0.7 T O 1. 3 Naca Rm L54a27 National Advisory Committee For Aeronautics Research Memorandum

[21] Saxena, S., Mahesha, G. T. and Srinivas, G. (2020): Recent aerodynamic performance evaluation of commercial and non-commercial vehicles. *Journal of Physics:* Conference Series, 1706(1). https://doi.org/10.1088/1742-6596/1706/1/012220

[22] Sebastian, J. J., Suryan, A. and Kim, H. D. (2016): Numerical analysis of hypersonic flow past blunt bodies with aerospikes. *Journal of Spacecraft and Rockets*, 53(4), 669–677. https://doi.org/10.2514/1.A33414

[23] Sheikh, N., Singh, S. N., Veeravalli, S. V. and Hegde, S. (2020): Effect of Reynolds number and boundary layer thickness on the performance of V-cone flowmeter using CFD. *Flow Measurement and Instrumentation*, 73. https://doi.org/10.1016/j.flowmeasinst.2020.101728

[24] Sims, W. H., Boylan, D. E. and Hahn, J. S. (1965): Drag on blunt bodies with and without spikes in low-density hypersonic flow. *AIAA Journal*, 3(2), 365–366. https://doi.org/10.2514/3.2863.

[25] Srinivas, G., and Potti, S. R. (2014): Computational analysis of fighter aircraft wing under Mach number 0.7 for small sweep angles. *Applied Mechanics and Materials*, 592–594, 1020–1024. https://doi.org/10.4028/www.scientific.net/AMM.592-594.1020

[26] Srinivas, G. and Prakash, M. V. S. (2017): Aerodynamics and flow characterisation of multistage rockets. IOP Conference Series: Materials Science and Engineering, 197(1). https://doi.org/10.1088/1757-899X/197/1/012077

[27] R. Yadav and U. Guven. (2013): Aerothermodynamics of a hypersonic projectile with a double-disk aerospike. *Aeronautical Journal*, 117(1195), 913.

[28] Yamauchi, M., Fujii, K. and Higashino, F. (1995). Numerical investigation of supersonic flows around a spiked blunt body. *Journal of Spacecraft and Rockets*, 32(1), 32–42. https://doi.org/10.2514/3.26571

[29] Aakash, K., Aditya, A. and Srinivas, G. (2019): Recent developments of modern avionic systems in aeronautical applications. *Journal of Advanced Research in Dynamical and Control Systems*, 11(12 Special Issue), 923-929. doi:10.5373/JARDCS/V11SP12/20193294.